Modeling of scattering and depolarizing electro-optic devices. II. Device simulation

Paul E. Shames, Pang Chen Sun, and Yeshaiahu Fainman

We describe a simple method for performing accurate computer simulation and modeling of arbitrary-geometry electro-optic (EO) devices. We use a material EO model that includes the effects of scattering and depolarization as well as the change in the index of refraction. Finite-element analysis is used to determine the electrostatic field distribution for EO device designs. Attenuation of the transmitted light intensity as a result of scattering is modeled as an exponential function, and the intensity of transmitted depolarized light is shown to be a function of the scattering intensity. The total optical transmittance is determined by integration of these values over all the elements in the path of the propagating light. Lanthanum-modified lead zirconate titanate-based surface-electrode and transverse-electrode EO devices are designed and fabricated. Their experimentally measured performance is found to be in excellent agreement with our computer-simulation results.

OCIS codes: 160.2100, 190.5890, 230.2090.

1. Introduction

Electro-optic (EO) phase-modulation and switching devices based on weakly scattering[1] materials, such as lanthanum-modified lead zirconate titanate (PLZT), are traditionally designed by use of surface electrodes on thin wafers.[2,3] For most applications scattering is considered negligible, and device performance is modeled by use of a simple Jones calculus.[4–9] However, particularly for applications requiring large phase modulation,[10–14] strong applied electric fields can significantly increase scattering.[15] Additionally, these materials can exhibit depolarization caused by complex scattering processes in the PLZT material.[16] The traditionally used Jones calculus is not appropriate for modeling such devices, and in part I of this two-paper series (see pp. 3717–3725; this issue) we described[17] the necessity of using a more complicated polarization ray-tracing algorithm,[18] such as Stokes vectors and Mueller matrices. It was shown how such EO materials could be described accurately by use of the Mueller matrix coefficients of scattering, depolarization, and phase.

In this paper we describe a simple method for performing accurate computer simulation and modeling of arbitrary-geometry EO devices. Our method includes the effects of scattering, depolarization, and change in the index of refraction. In Section 2 a general method for simulating EO-device performance is presented. Finite-element analysis (FEA) is used to calculate the electric-field distribution for irregularly shaped devices as well as to determine the change in phase, attenuation, and depolarization for light propagating through EO materials that exhibit scattering. The application of this method to specific devices based on the EO material PLZT is discussed in Section 3. Two example geometries that use surface or transverse electrodes are modeled, and the computer simulations of device performance are compared with the experimentally measured performance of fabricated devices. Finally, in Section 4 the advantages and limitations of our modeling technique and our conclusions are presented.

2. General Methodology for Modeling Electro-Optic Devices

Our method of incorporating the effects of scattering and depolarization into EO-device modeling begins with the determination of the electric-field distribution for a given device geometry. Such device models require the input of material electrical properties and applied voltages. Our FEA calculations subdivide the device domain into multiple elements (i.e., subdomains), for which the electric-field distributions are easily calculated. Combining this distribution

The authors are with the Department of Electrical and Computer Engineering, University of California, San Diego, 9500 Gilman Drive, La Jolla, California 92093-0407.

Received 13 October 1997.
0003-6935/98/03726-09$15.00/0

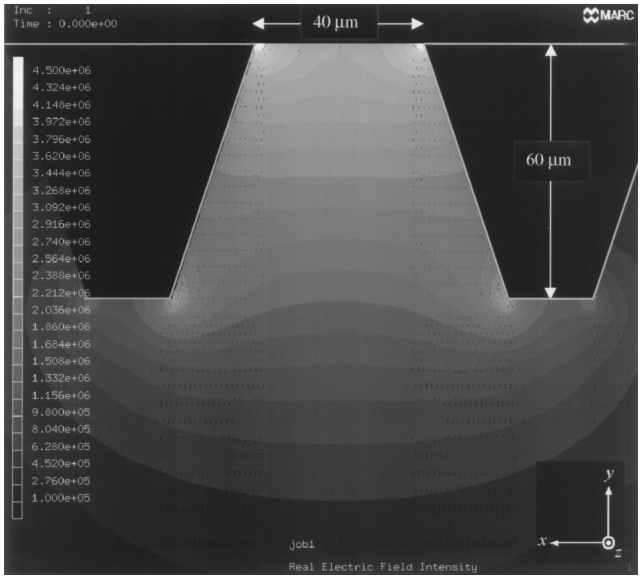

Fig. 1. FEA-calculated electric-field strength distribution for trapezoid-shaped embedded electrodes separated by 40 and 60 μm, with a potential difference of 124 V.

data with electric-field-induced material properties, such as the EO effect and scattering, allows the optical response of the material to be determined within each finite element, i.e., as a function of position within the device. The EO response of the material varies the local index of refraction, represented by an index ellipsoid, which is used to determine the change in phase for light passing through the material. Electric-field-induced scattering attenuates the transmitted light and can also cause depolarization. Assuming the attenuation has a simple exponential dependence on the propagation distance, we incorporate the scattering and the depolarization into our EO model. By integration of these responses along a path through multiple finite elements, an accurate optical response for the entire device can be calculated.

A. Finite-Element Analysis for Calculation of the Electric-Field Distribution

FEA is a useful technique for calculations of electric-field distributions in devices with arbitrary geometries. For instance, the use of embedded electrodes can significantly improve the performance of devices based on the use of thin-wafer EO substrates.[8] Varying the geometry of the electrodes also allows the phase profile of the modulated optical wave to be controlled.[19] Furthermore, optimization of device performance could require the use of nonrectangular-electrode geometries. For example, we find that by using trapezoidal-shaped electrodes (see Fig. 1) an incident plane wave can maintain its wave-front uniformity after passing through the EO device. However, it can be very difficult to calculate the electric-field distribution for electrodes with arbitrary geometries by use of analytic methods. One numerical-approximation method is to subdivide the device (or domain) into many parts (subdomains) within which the field can be more easily calculated.[20] For low-frequency applied field devices an *electrostatic* FEA model can be used in which each subdomain is defined by a geometric element having a given set of material properties (e.g., permittivity) and boundary conditions (fixed potential, charge, etc.). For high-frequency applications an *electrodynamic* FEA model, which can account for the time-dependent material responses, is used. One advantage of the FEA method is that there exists a large selection of finite-element types and shapes that allow for the generation of a finite-element mesh that provides a good fit for any device geometry.

The FEA calculations and postprocessing for this project were performed with MARCK6 and MENTAT software from Marc Analysis, Inc. The orthogonal components of the electric field, E_x, E_y, and E_z, are calculated at integration points near the nodes (corners) of the elements. Figure 1, a two-dimensional (2-D) cross section of a device with trapezoid-shaped embedded electrodes, shows a contour plot of the magnitude of the electric field given by

$$E = (E_x^{\,2} + E_y^{\,2} + E_z^{\,2})^{1/2}, \tag{1}$$

where values between integration points are found by interpolation. For calculating phase modulation and phase scattering (discussed below), our modeling technique calls for a constant electric field within each element, which is found when the average of the integration-point values is taken. In regions with steep potential gradients (e.g., near the corners of electrodes) the finite-element mesh must be refined, i.e., the elements are subdivided to increase the mesh density, for good accuracy of the electric-field calculations. For the 2-D models described in this paper, we use of the order of 10^3 elements, which provides an electric field accuracy to within 5% of those values calculated by use of analytic methods.[21,22]

B. Index Ellipsoid and Change of Phase

Consider a monochromatic plane wave propagating in an arbitrary direction through an anisotropic crystal; two independent, linearly polarized, propagation modes can exist whose phase velocities are determined by the indices of refraction n_A and n_B along each direction of polarization.[23] The intersection of the material's index ellipsoid[24]

$$\frac{x^2}{n_x^{\,2}} + \frac{y^2}{n_y^{\,2}} + \frac{z^2}{n_z^{\,2}} = 1 \tag{2}$$

and the plane normal to the direction of propagation produce an ellipse whose major and minor semi-axes determine the indices n_A and n_B. For EO materials these indices depend on the strength and direction of an applied electric field.[25]

For EO devices that exhibit nonuniform electric fields the index ellipsoid can vary as a function of position. If the index variation is negligibly small over a distance of the order of a wavelength, the

phase for each polarization component can be expressed by the eikonal equation

$$\phi(\mathbf{r}) = \frac{2\pi}{\lambda} \int n(\mathbf{r}) \mathrm{d}s, \tag{3}$$

where the integration is taken along the propagation path.[26] In this paper we assume that the electric field is piecewise constant. That is, within each element there exist a constant electric-field strength and direction. Therefore, for each element, the index ellipsoid is constant as a function of position, and the phase for each propagating orthogonal-polarization component is given by

$$\phi_k = \frac{2\pi}{\lambda} n_k L, \tag{4}$$

where the subscript k indicates one of the two possible orthogonal polarizations (i.e., $k = A, B$), n_k is the associated index of refraction for each orthogonal-polarization direction within an element, λ is the wavelength of the light, and L is the propagation distance in the element. Since the finite-element shapes used are arbitrarily chosen, we ignore any change in propagation direction that is due to index variation at element boundaries (i.e., the Snell law). Therefore, for light passing through N elements, i.e., through a device, the total phase is

$$\phi_k = \frac{2\pi}{\lambda} \sum_{i=1}^{N} n_{k_i} L_i, \tag{5}$$

where n_{k_i} and L_i can vary for each element. For the determination of transmission intensity we are interested in the phase difference between the two orthogonal-polarization components; this difference is given by

$$\Delta\phi = \frac{2\pi}{\lambda} \sum_{i=1}^{N} \Delta n_i L_i, \tag{6}$$

where $\Delta n \equiv |n_A - n_B|$.

C. Attenuation, Depolarization, and Transmission Intensity

For materials that have electric-field-induced scattering, the transmitted light intensity will be attenuated as a function of the electric field. In general, we can consider such materials to be lossy and model them by using[15]

$$A = A_0 \exp[-\alpha(E) L], \tag{7}$$

where A is the transmitted light intensity, A_0 is the incident intensity, α is the attenuation coefficient and is a function of the electric-field magnitude, and L is again the propagation length. The specific form of the scattering will depend on the material and on the strength of the applied electric field. For example, PLZT can be modeled as a random distribution of single-particle scatterers[15] for which the attenuation coefficient is a function of wavelength and scattering-center size. For materials with anisotropic scattering, the intensity of the second orthogonal-polarization component, denoted by B, can differ and is given by

$$B = B_0 \exp[-\beta(E) L], \tag{8}$$

where B_0 is the incident intensity and β is the attenuation coefficient. In our FEA model, Eqs. (7) and (8) describe the attenuation that is due to scattering within a single element. For light passing through multiple elements the nonscattered polarization-component intensity from one element will be attenuated by the following element, i.e., $A_2 = A_1 \exp[-\alpha(E)_2 L_2]$. Therefore for light propagating through N elements the total scattering for the two polarization components is given by

$$A = A_0 \prod_{i=1}^{N} \exp[-\alpha(E)_i L_i] = A_0 \exp\left[-\sum_{i=1}^{N} \alpha(E)_i L_i\right], \tag{9}$$

$$B = B_0 \prod_{i=1}^{N} \exp[-\beta(E)_i L_i] = B_0 \exp\left[-\sum_{i=1}^{N} \beta(E)_i L_i\right]. \tag{10}$$

For certain EO materials the scattered light will have random polarization, i.e., will produce unpolarized light.[27] We use the term depolarized to refer to that portion of this scattered light that remains within the solid angle of an optical system and is detected. For determining the existence of depolarized light in a system, the angle of an analyzer (a polarizer situated after the EO device) can be rotated to block the transmitted polarized light.[17] The remaining detected light intensity represents half of the total depolarized light.

The depolarized light intensity U can be described as a function of S, the scattered light intensity, i.e., $U = f(S)$. The total scattered light in each orthogonal-polarization direction is simply the difference between the total incident light A_0 and the intensity of the polarized light A, i.e., $S = A_0 - A$; therefore

$$U = f(A_0 - A), \tag{11}$$

where any loss of intensity caused by absorption is included in the scattering term. For materials with anisotropic scattering the intensity of the depolarized light will be a function of the two orthogonally polarized light components. The depolarized light intensity measured in one polarization direction could be due to scattering of either polarization component. The specific form of the function will depend on the EO material properties.

Equation (11) describes the depolarization intensity as a function dependent on the orthogonally polarized light-intensity coefficient A, making no distinction between the depolarization for light propagating through elements with specific electric-field strengths or propagation lengths. By examining Eq.

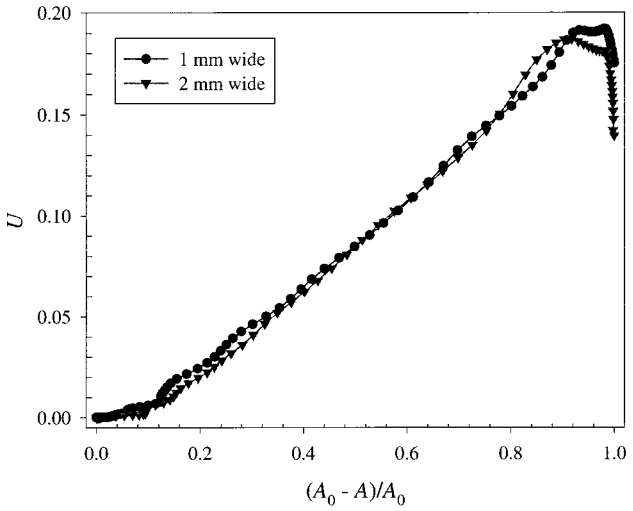

Fig. 2. Depolarized light (normalized) intensity as a function of the polarized-light intensity for identical PLZT samples with propagation lengths of 1 and 2 mm.

(7), we can see that the polarized light intensity A is dependent on the *product* of these two factors and is therefore not unique. To confirm the accuracy of this description, we measured the attenuation caused by scattering A and the intensity of the depolarized light U as functions of the applied electric-field strength in two samples of PLZT 9.0/65/35, for which one sample was twice the thickness (i.e., propagation length) of the other. In Fig. 2 we plot U as a function of $(A_0 - A)/A_0$ and observe that the two cases are practically identical, which is consistent with Eqs. (7) and (11), which predict that the two should be indistinguishable.

By use of Stokes vectors and Mueller matrices, the transmitted intensity for normally incident light passing through an optical system comprising a linear polarizer, an EO device, and an analyzer can be found in terms of the change in phase between two orthogonally polarized components and the intensity of the polarized-light and the depolarized-light components.[17] For a crossed polarizer and analyzer pair oriented at 45° with respect to the two orthogonal-polarization directions, the transmitted optical intensity is

$$I_{45°,45°} = \frac{1}{4}\{A + B + U_{AA} + U_{AB} + U_{BB} + U_{BA} - 2\sqrt{AB}\cos(\Delta\phi)\}. \quad (12)$$

For materials that exhibit isotropic scattering, Eq. (12) reduces to

$$I_{45°,45°} = \frac{1}{2}\{A + 2U - A\cos(\Delta\phi)\}. \quad (13)$$

In Section 3 we discuss modeling two such devices and compare the numerically predicted results with experimentally measured performances of fabricated devices.

3. Examples: Electro-Optic Devices

The modeling method described in Section 2 can be applied to a general class of scattering and depolarizing EO devices that have nonuniform electric fields that can vary in all three directions. However, EO devices often exhibit translational symmetry, which can be modeled by use of 2-D cross sections. In this section we discuss two representative device geometries that have such symmetry: (i) long and narrow surface electrodes with which the incident light is normal to the surface [see Fig. 3(a)] and (ii) transverse electrodes that are placed on opposing surfaces of an EO crystal with which the incident light is normal to the edge of the EO material [see Fig. 3(b)].

A. Surface-Electrode Geometry

For surface- or embedded-electrode geometries the electrode length is generally much greater than the width, and it can be assumed that there is a negligible field component parallel to the electrode length, i.e., $E_z \approx 0$. Therefore the electric field can be modeled by a 2-D cross section (x–y plane) perpendicular to the electrodes (see Fig. 4), where the strength and direction of the field vary as functions of position in

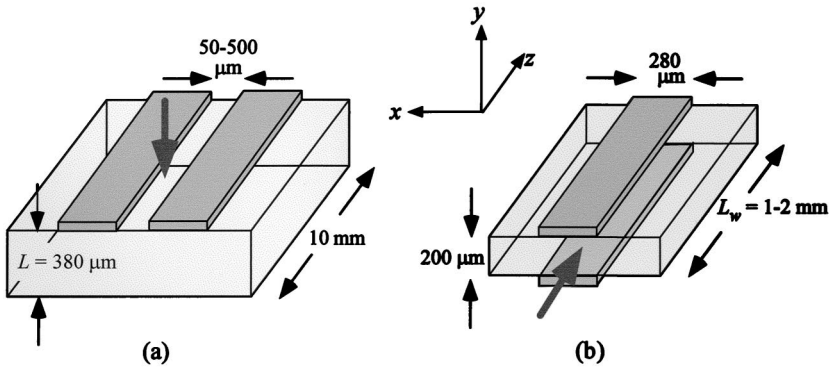

Fig. 3. (a) Surface-electrode device in which CrAu electrodes are evaporated onto the surface of the PLZT wafer and light is normally incident on the surface (along the y axis). (b) Transverse-electrode device in which electrodes are on opposite sides of the wafer and light is normally incident on the polished edges (along the z axis).

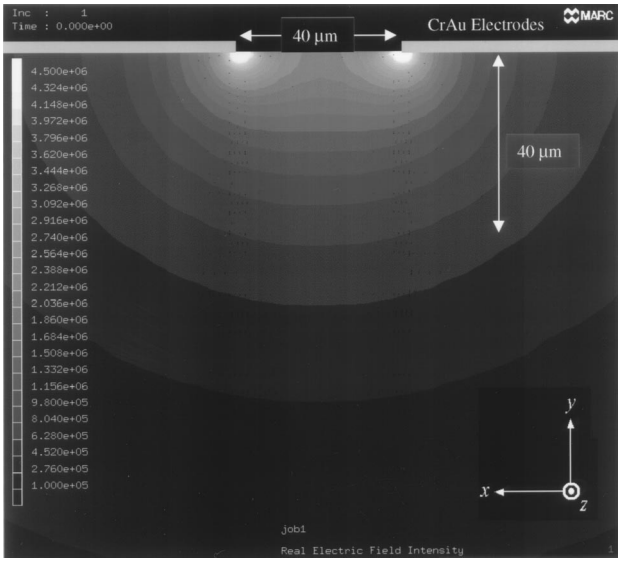

Fig. 4. Two-dimensional cross section of the electric-field strength distribution within PLZT for a surface-electrode device with electrodes separated by 40 μm and a potential difference of 124 V. Charge buildup at the corners of the electrodes results in a large gradient of the electric field within the electrode gap near the surface of the device.

the device. In these devices the optical beam is normally incident on the surface of the device and propagates along the y axis. Therefore the plane normal to the direction of propagation is parallel to the x–z plane of the device.

Under an applied electric field, polycrystalline PLZT is usually modeled as a uniaxial crystal[1] with the principal index ellipsoid given by[23]

$$\frac{x'^2}{n_e^2} + \frac{y'^2}{n_o^2} + \frac{z'^2}{n_o^2} = 1, \tag{14}$$

where the principal axes are denoted by x', y', and z'. The intersection of the normal plane for an incident linearly polarized plane wave has indices of refraction given by

$$n_A = n_z = n_o, \tag{15}$$

$$n_B = n_x = \left\{ \frac{\cos^2[\theta(x,y)]}{n_e^2} + \frac{\sin^2[\theta(x,y)]}{n_o^2} \right\}^{-1/2}, \tag{16}$$

where the extraordinary index n_e is in the direction of the electric field,[8] the ordinary index n_o is perpendicular to the field, and $\theta(x,y) = \tan^{-1}\{[E_y(x,y)]/[E_x(x,y)]\}$ defines the direction of the field (see Fig. 5).

We define the extraordinary index of refraction in terms of the change relative to the ordinary index and the applied electric-field strength, i.e.,

$$n_e = n_o - \Delta n_{\text{meas}}(E), \tag{17}$$

where $\Delta n_{\text{meas}}(E)$ was determined experimentally.[17] For PLZT 9.0/65/35 the change in the extraordinary index of refraction is much greater than the change in the ordinary index[1]; therefore we take n_o as a constant value of 2.5 (equal to the isotropic index[28]). For incident light whose polarization direction is oriented at 45° with respect to the direction of the electrodes, i.e., in the x–z plane, we find the relative change in the index of refraction between the x- and z-polarization components for each finite element to be

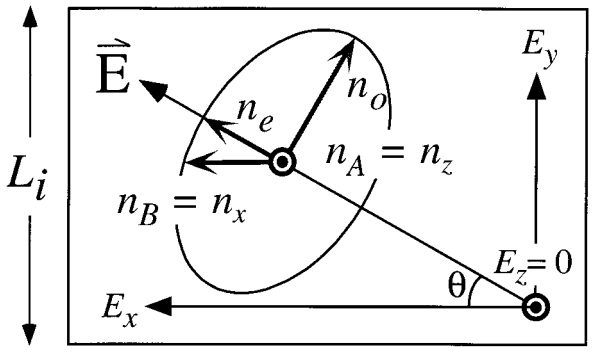

Fig. 5. Single element of the 2-D cross section where we calculate an average electric-field magnitude and direction. We show the variation of the index ellipse following the direction of the electric field.

$$\Delta n = |n_x(E) - n_z|, \tag{18}$$

and the change in phase for the device is then found with Eq. (6).

The experimentally characterized PLZT 9.0/65/35 exhibited negligible anisotropic scattering and can be assumed to have isotropic scattering. Substituting the experimental data for the attenuation,[17] $A_{\text{meas}}(E)$ as a function of electric-field strength, in Eq. (7) and solving for the attenuation coefficient, we get

$$-\alpha = \frac{1}{L}\left[\ln \frac{A_0}{A_{\text{meas}}(E)} \right]. \tag{19}$$

The total attenuation of a polarization component propagating through the device is found by substitution of Eq. (19) into Eq. (9) for each element along an optical beam path, producing

$$A = A_0 \prod_{i=1}^{N} \left[\frac{A_{\text{meas}}(E_i)}{A_0} \right]^{L_i/L}. \tag{20}$$

The depolarized light intensity is found by use of the attenuated intensity from Eq. (20) and the depolarization function from the experimental data shown in Fig. 2. Substituting the calculated phase as well as the intensity of the polarized and depolarized components of the light into Eq. (13) produces a set of intensity values for each column or path of elements across the electrode gap.

To compare computer simulations with the performance of a real device, we fabricated a surface-electrode device on a PLZT 9.0/65/35 wafer 380 μm thick, with 2-mm-wide CrAu electrodes spaced 500 μm apart. The device is placed between crossed dichroic polarizers aligned at 45° with respect to the surface-electrode length direction and illuminated

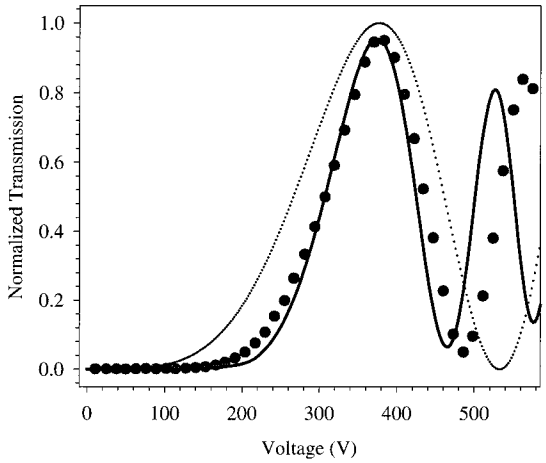

Fig. 6. Simulation (solid curve) of the surface-electrode device performance, with an electrode gap of 500 μm for PLZT 9.0/65/35 that is 388 μm thick, and experimental data for a fabricated device (circles) in comparison with the simulation results (dotted curve) with the commonly employed Jones calculus and quadratic EO model.

with a He–Ne laser (see also Fig. 3 in Ref. 17). The transmitted optical intensity is detected by use of an optical power meter (Newport, Model 835). A slit aperture in the detector plane is used to sample only the central 100-μm area of the gap (to avoid the effects of space-charge fields[29] at electrode edges). The resultant intensity measurement is an average of the values found across the center of the gap. The experimentally measured transmitted intensity is plotted as a function of the applied voltage in Fig. 6 (circles).

Using an identical device geometry, we simulate the transmitted optical intensity, for which we also use the average transmittance across the 100-μm center section of the electrode gap. For simulations of a device that uses PLZT 9.0/65/35, the published quadratic EO coefficient,[1] $R = 3.0 \times 10^{-16}$ $(\mathrm{v/m})^2$, produces results that do not coincide at all with our experimental data. Therefore we used a best fit to the first maximum, which gives $R = 5.0 \times 10^{-16}$ $(\mathrm{V/m})^2$. In Fig. 6 we show the simulation by using the traditional Jones calculus and quadratic EO-effect model[4–9] (dotted curve). The traditional model that uses the best-fit EO coefficient still fails to follow the variation of the phase as a function of voltage accurately. Also, since scattering and depolarization effects have not been accounted for, this simulation incorrectly predicts the intensities of the maxima and minima values.

The simulation that uses our new model, which incorporates the Mueller matrix coefficients for attenuation and depolarization as well as the experimentally determined EO function, is also shown in Fig. 6 (solid curve). Here we observe that the new model correctly predicts the flat response at low voltage as well as the attenuation caused by scattering losses of the maximum and the increase in the minimum intensity caused by depolarization. The sinusoidal variation of the optical intensity is due to the EO phase modulation. Our model successfully describes this change of phase, within the error of our FEA model, up to $V_{2\pi}$.

At higher voltages, our model predicts electric-field strengths well above the EO characterization data. Since the simulation predicts a greater phase change than is observed experimentally, we can conclude that there are significant variations in the EO response under such high fields. These variations may be due to surface effects[28] as well as to a stored space-charge field[29,30] near the electrode–PLZT interface. In previous studies, geometry and high-field-dependent effects were accounted for by use of a variable coefficient[5] in the phase-change calculation. However, to improve the accuracy of modeling under very high fields, a more accurate model of the material EO response as well as of the device-dependent electric-field effects is required.

Surface-electrode devices generally have strong transverse electric-field strengths near the surface that quickly drop off to negligible values within a distance of tens of micrometers into the substrate (see Fig. 4). Since phase modulation is directly dependent on the transverse field, this limits the effective EO propagation length. Therefore high applied voltages are often necessary to achieve a required phase modulation. Embedded-electrode devices can increase the penetration depth of the electric field, resulting in far lower voltage requirements (see Fig. 1). However, the fabrication of such devices can be quite difficult.[8] An alternative design is to use a transverse-electrode geometry, as discussed in Subsection 3.B.

B. Transverse-Electrode Geometry

In a transverse-electrode geometry the electrodes are applied on the top and the bottom of a wafer, and the light is normally incident on the polished wafer edges [see Fig. 3(b)]. The voltage gradient is now almost completely in the y direction, resulting in a strong transverse field for light propagating along the z axis. For devices in which the electrode length (z direction) is much longer than the width (x direction), the electric-field component along the z axis will be negligible, i.e., $E_z \approx 0$ (ignoring fringing fields). Taking advantage of this translational symmetry along the z axis, we use a 2-D cross section in the x–y plane to model the electric-field distribution.

For linearly polarized light propagating along the z axis, the polarization index of refraction along the z axis is given by Eq. (16), and the orthogonal-polarization index along the y axis is

$$n_A = n_y = \left\{ \frac{\sin^2[\theta(x,y)]}{{n_e}^2} + \frac{\cos^2[\theta(x,y)]}{{n_o}^2} \right\}^{-1/2}. \quad (21)$$

Again we can describe the extraordinary index of refraction in terms of the change in the ordinary index by using Eq. (17) and find the change in the index

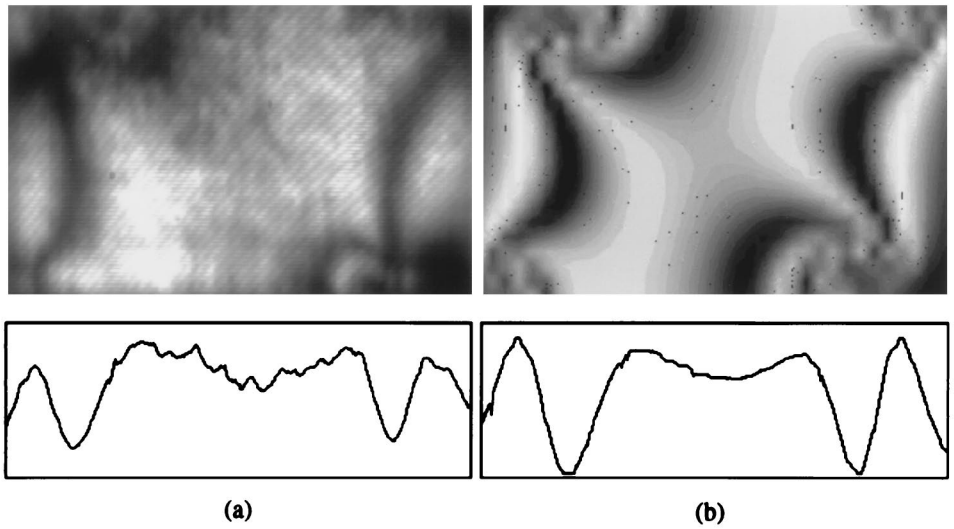

Fig. 7. (a) Experimentally measured CCD image for a transverse-electrode device with 280-μm electrodes separated by 200 μm of PLZT 9.0/65/35 with an applied voltage of 98 V. The interaction length, i.e., thickness of PLZT, is 1 mm. The diagonal fringe pattern is due to the glass cover plate on the CCD camera. (b) Computer-simulated intensity by use of identical electrode geometry. The black dots are remnants of the PostScript rendering. Below each image is an intensity profile taken across the center of the image.

of refraction between the two orthogonal-polarization components,

$$\Delta n = |n_x(E) - n_y(E)|, \tag{22}$$

as a function of the electric-field strength and direction.

Since the field is assumed to be constant along the z axis, the change in phase for light propagating through the device is simply given by

$$\Delta\phi(x, y) = \frac{2\pi}{\lambda}\,\Delta n(x, y) L_w, \tag{23}$$

where the propagation length L_w is the width of the device in the z direction. Here we have defined the change in phase explicitly as a function of position in the x–y plane, indicating that the change in phase depends on the electric-field strength and direction at every point in the plane. The attenuation equation [Eq. (7)] simplifies to

$$A(x, y) = \left[\frac{A_{\text{meas}}(E)}{A_0}\right]^{L_w/L} \tag{24}$$

for every point in the x–y plane, and the depolarization is again defined by the function shown in Fig. 2. The optical transmittance for the device placed between crossed polarizers oriented at 45° with respect to the electrodes (x–y axes) is found by substitution of these values into Eq. (13).

For a comparison of the simulated performance of a transverse-electrode device with a fabricated device we examine the variation of the EO response as a function of position across the entire electrode gap (i.e., the polished edge of the device). We fabricated a transverse-electrode device in which 280-μm-wide CrAu electrodes were applied to the top and the bottom of a 200-μm-thick and 1-mm-long PLZT 9.0/65/35 wafer (see Fig. 3). The light is transmitted through the polished edges and crossed polarizers set at 45° relative to the electrodes. The output light is imaged onto a CCD camera. To avoid speckle noise, we employ an incoherent imaging system, which uses He–Ne 633-nm laser light converted into spatially incoherent light by use of a rotating ground glass.

A CCD image of the fabricated device that uses an applied voltage of 98 V is shown in Fig. 7(a). Because of charge buildup at the corners of the electrodes, there is a steep gradient of electric-field strength and index of refraction in those regions, which cause a variation of phase and transmitted intensity. As a result, we see a pattern of light and dark regions or fringes, whose maxima and minima represent multiples of $2n\pi$ and $(2n + 1)\pi$ phase, respectively, where n is an integer. We see a slight asymmetry of the fringe pattern, which is due to a fabrication error that resulted in the opposing electrodes being misaligned by 40 μm.

For computer simulation of this device geometry we calculate the transmission intensity as a function of x–y position between the electrodes by using the same geometry (i.e., misalignment) and potential difference as the fabricated device [Fig. 7(b)]. A subjective comparison of the two images (fabricated and simulated devices) shows a good match for the light and dark fringe patterns. Below each image is a plot of the intensity profile taken across the centers of both images. The positions of the maxima and minima (i.e., fringes) are almost identical. The minima (i.e., dark regions) intensities are slightly different, which is probably due to background noise within the CCD camera and scattering effects not accounted for in our model.

A more objective comparison is shown in Fig. 8,

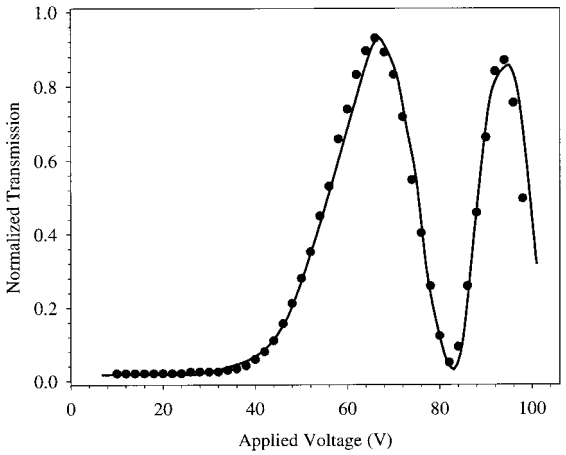

Fig. 8. Experimental data (circles) and simulated results (curve) of transmission through the central 20 μm × 20 μm area of the transverse-electrode device with 280-μm electrodes separated by 200 μm of PLZT 9.0/65/35 [see Figs. 7(a) and 7(b)].

where we compare the experimental data and simulated results for an average transmission for a region 20 μm × 20 μm in the center of the transverse-electrode device. The results indicate an excellent match between the measured data and the simulated results for as high as a 3π phase shift (i.e., the second maxima). Under an applied voltage of 100 V the electric-field strength in the center of the device is approximately 5×10^6 (V/m), which indicates that for this device design our model is accurate into the EO saturation region of the PLZT material used.

4. Conclusion

In this paper we have described a simple method for performing accurate computer simulation and modeling of arbitrary-geometry EO devices. Our method includes the effects of scattering, depolarization, and change in the index of refraction. PLZT-based surface-electrode and transverse-electrode EO devices have been designed, fabricated, and experimentally tested. Our isotropic-scattering model produced an excellent correlation between the measured performance of the fabricated devices versus that predicted by our simulations. For surface-electrode devices we were able to predict accurately the transmission intensity of light up to a 2π phase variation. For the transverse-electrode device our model was accurate up to a 3π phase variation. A simulation of a cross section of the transverse-electrode device shows the large degree of phase variation that can occur within an electrode gap for finite-sized electrodes. We are currently using these simulation techniques to optimize device design for a variety of applications and performance characteristics, including maximum contrast, efficiency, and minimized cross talk in array devices.

In these calculations of an optical beam passing through an optical system we have assumed that the variation of the index of refraction is very small within each element and that we can calculate the change in phase on the basis of a constant index within each element. For regions near the corners of the electrodes this is not an accurate assumption. However, the regions of steep gradient are very small and have a minimal effect on the total phase change or beam-propagation direction. We have considered only the interaction length of each element in calculating the change in relative phase and the intensity of the beam. That is, we have assumed a plane wave that experiences no diffraction. We have also assumed that each ray has a vector component along the direction of propagation only, and therefore there is no interaction between rays. To include diffraction or scalar effects, it would be necessary to have a more precise model, such as rigorous coupled-wave analysis.[31]

The authors appreciate the useful discussions with Rong-Chung Tyan and James Thomas at the University of California, San Diego. We also thank Eddie Rezler from Marc Analysis for support in the development of our computer simulations. This study was funded in part by the National Science Foundation, the Air Force Office of Scientific Research, and Rome Laboratories.

References

1. G. Haertling, "Electro-optic ceramics and devices," in *Electronic Ceramics: Properties, Devices and Applications*, L. Levinson, ed. (Marcel Dekker, New York, 1988), pp. 371–492.
2. J. T. Cutchen, J. O. Harris, and G. R. Laguna, "PLZT electro-optic shutters: applications," Appl. Opt. **14,** 1866–1873 (1975).
3. T. Utsunomiya, "Optical switch using PLZT ceramics," Ferroelectrics **109,** 235–240 (1990).
4. R. Viennet, "Driving voltage calculation for a ferroelectric display device," J. Math. Phys. Appl. **29,** 715–722 (1978).
5. E. E. Klotin'sh, Yu. Ya. Kotleris, and Ya. A. Seglin'sh, "Geometrical optics of an electrically controlled phase plate made of PLZT-10 ferroelectric ceramic," Avtometriya **6,** 68–72 (1984).
6. K. Tanaka, M. Yamaguchi, H. Seto, M. Murata, and K. Wakino, "Analyses of PLZT electro-optic shutter and shutter array," Jpn. J. Appl. Phys. **24,** 177–182 (1985).
7. A. R. Dias, R. F. Kalman, J. W. Goodman, and A. A. Sawchuck, "Fiber-optic crossbar switch with broadcast capability," Opt. Eng. **27,** 955–960 (1988).
8. M. Title and S. H. Lee, "Modeling and characterization of embedded electrode performance in transverse electrooptic modulators," Appl. Opt. **29,** 85–98 (1990).
9. A. Y. Wu, T. C. Chen, and H. Y. Chen, "Model of electro-optic effects by Green's function and summary representation: applications to bulk and thin film PLZT displays and spatial light modulators," in *Proceedings of the Eighth IEEE International Symposium on Applications of Ferroelectrics*, M. Liu, A. Safari, A. Kingon, and G. Haertling, eds. (Institute of Electrical and Electronics Engineers, New York, 1992), pp. 600–603.
10. F. S. Chen, "Evaluation of PLZT ceramics for application in optical communications," Opt. Commun. **6,** 297–300 (1972).
11. J. Thomas and Y. Fainman, "Programmable diffractive optical elements using a multichannel lanthanum-modified lead zirconate titanate phase modulator," Opt. Lett. **20,** 1510–1512 (1995).
12. Q. W. Song, X. M. Wang, and R. Bussjager, "Lanthanum-modified lead zirconate titanate ceramic wafer-based electro-optic dynamic diverging lens," Opt. Lett. **21,** 242–244 (1996).

13. Q. W. Song, P. J. Talbot, and J. H. Maurice, "PLZT based high-efficiency electro-optic grating for optical switching," J. Mod. Opt. **41,** 717–727 (1994).
14. F. Castro and B. Nabet, "Design of dual-effect lens on lanthanum-modified lead zirconate titanate for continuous variation of focal length," Appl. Opt. **34,** 2317–2323 (1995).
15. M. Ivey and V. W. Bolie, "Birefringent light scattering in PLZT ceramics," IEEE Trans. Ultrason. Ferroelectr. Freq. Contr. **38,** 579–584 (1991).
16. C. E. Land, "Variable birefringence, light scattering, and surface-deformation effects in PLZT ceramics," Ferroelectrics **7,** 45–51 (1974).
17. P. E. Shames, P. C. Sun, and Y. Fainman, "Modeling of scattering and depolarizing electro-optic devices. I. Characterization of lanthanum-modified lead zirconate titanate," Appl. Opt. **37,** 3717–3725 (1998).
18. R. A. Chipman, "The mechanics of polarization ray tracing," in *Polarization Analysis and Measurement*, D. H. Goldstein and R. A. Chipman, eds., Proc. SPIE **1746,** 62–75 (1992).
19. P. Shames, P. C. Sun, and Y. Fainman, "Modeling and optimization of electro-optic phase modulator," in *Physics and Simulation of Optoelectronic Devices IV*, W. W. Chow and M. Osinski, eds., Proc. SPIE **2693,** 787–796 (1996).
20. J. Jin, *The Finite Element Method in Electromagnetics* (Wiley, New York, 1993), Chap. 2.
21. Y. Yeh and Q. Zeng, "Exact solution to the electric field of the double-sided electrode structure in a lead lanthanum zirconate titanate transverse electro-optic modulator," Opt. Lett. **21,** 961–963 (1996).
22. H. Engan, "Excitation of elastic surface waves by spatial harmonics of interdigital transducers," IEEE Trans. Electron. Devices **16,** 1014–1017 (1969).
23. A. Yariv and P. Yeh, *Optical Waves in Crystals* (Wiley, New York, 1984), Chap. 5.
24. A. Yariv, *Quantum Electronics* (Wiley, New York, 1989), Chap. 5.
25. J. F. Nye, *Physical Properties of Crystals* (Clarendon, London, 1985), Chap. 2.
26. R. Boyd, *Nonlinear Optics* (Academic, Boston, 1992), Chap. 7.
27. A. L. Dalisa and R. J. Seymour, "Convolution scattering model for ferroelectric ceramics and other display media," Proc. IEEE **61,** 981–991 (1973).
28. P. D. Thacher, "Refractive index and surface layers of ceramic $(Pb,La)(Zr,Ti)O_3$," Appl. Opt. **16,** 3210–3213 (1977).
29. P. J. Chen, C. E. Land, and M. M. Madsen, "A theory of the influence of space-charge field on domain switching in PLZT 7/65/35 ceramic," Acta Mechan. **43,** 61–72 (1982).
30. C. E. Land, "Effects of photoferroelectric space charge fields on visible-light scattering in PLZT ceramics," Ferroelectrics **27,** 143–146 (1980).
31. F. Xu, R. C. Tyan, P. C. Sun, Y. Fainman, "Fabrication, modeling and characterization of form-birefringent nanostructures," Opt. Lett. **20,** 2457–2459 (1995).